Hindawi

Research Article

Numerical Simulation of Acoustic Emission Events in Supporting Roadways under Different Dynamic Loads

Wenzheng Shang [ID],[1] **Zhigang Liu** [ID],[1,2,3] **Jianbo Yuan,**[1] **Wuchao You,**[4] **Shuai Han,**[4] **Lei Yu,**[4] **and Shihua Zhang**[3]

[1]*Institute of Mining Engineering, Shandong University of Science and Technology, Tai'an 271019, China*
[2]*Shandong Energy Group, Jinan 250013, China*
[3]*A Key Laboratory of Deep Coal Resource Mining, School of Mines, Ministry of Education of China,*
 China University of Mining and Technology, Xuzhou 221116, China
[4]*Shandong Jingtai Engineering Technology Co., Ltd., Zibo 255425, China*

Correspondence should be addressed to Zhigang Liu; 15865721818@163.com

This paper studies the distribution characteristics of acoustic emission (AE) events in supporting roadways under different dynamic load conditions through numerical simulation and theoretical analysis. According to the principle of AE numerical simulation, the roadway model is established by FLAC3D software, and the supporting structure of the bolt cable is established by editing the Fish function. According to the model dynamic load application criterion, the relationship between the peak velocity of the particle, the distance from the source center to the dynamic impact damage point, and the dynamic load intensity is introduced. The velocity-distance-energy relationship is deduced from the relationship to determine the magnitude of the dynamic load energy. The simulation results show that the intensity of the dynamic load source and the distance of the dynamic load source directly impact the AE events. The larger the dynamic load intensity and the closer to the dynamic load source, the more concentrated the AE events. The roadway has a blocking effect on the transmission of the dynamic load stress waves. According to this characteristic, the roadway can be protected by a high-pressure relief roadway. Rock lithology greatly influences the transmission of dynamic load stress waves and the number of AE events. When the dynamic load stress wave passes through the rock strata of different lithologies, the attenuation of the dynamic load energy and the number of AE events are large. However, when the dynamic load stress wave passes through the rock strata of the same lithology, the attenuation of the dynamic load energy and AE events is small. The surrounding rock structure in the bottom corner area of the roadway is susceptible to disturbance from dynamic load sources above the roadway. The results are greatly significant for studying the AE characteristics of support roadways with disturbance-typeimpact failure.

1. Introduction

With the deepening of coal mining, rock burst [1, 2] disasters have become increasingly serious, which seriously restricts the safe mining of coal. Due to the complexity of rock burst disaster-causing factors and the uncertainty of time and space, the current stage of rock burst research work cannot completely prevent or warn against disasters. As the last line of defense for the prevention and control of rock bursts, the support is affected by three highs and one disturbance effect [3–5]. Several dynamic stress phenomena in the mining process are likely to become factors of fracture and instability of the surrounding rock in the supporting roadway. Therefore, the support roadway faces new challenges. The disturbance-type shock failure of the roadway surrounding the rock source [6] has a great influence on roadway support design. The impact failure type of the source disturbance is accompanied by the transfer of energy, and the energy transmitted to the roadway in the form of waves damages the rocks around the roadway and along the energy propagation

path, resulting in rock fracture. The fracture damage of the rock releases elastic energy, resulting in acoustic emission (AE) events. Using AE detection technology [7, 8] and numerical simulation software to study the fracture characteristics of rock with source disturbance impact damage is of great significance for roadway support design.

For a long time, scholars worldwide have conducted several studies on applying AE-monitoring technology in coal mining. Based on the laboratory simulation test, Lin et al. [1] used the impact loading device to conduct loading and unloading tests on the surrounding rock model under four different stress gradients. By capturing the AE energy events of loading and unloading specimens and infrared monitoring anomalies, the energy evolution characteristics of the model during the entire loading process were quantitatively analyzed. Li et al. [9] conducted hydraulic fracturing (HF) tests under true triaxial stress on three-dimensional coal samples in the laboratory and studied the time variation of injection pressure curves and AE waveform parameters at different stages through AE-monitoring technology. The results showed that the characteristics of the AE waveform parameters well reflect the growth behavior of coal HF. Zhili et al. [10] studied the AE, energy, and damage evolution of coal samples under three uniaxial cyclic loading and unloading conditions. Based on the Brazilian-splitting test and uniaxial and triaxial compression tests, Su et al. [11] and Yang et al. [12], respectively, studied the evolution of rock failure and AE characteristics under different loading rates, which further deepened the understanding of rock failure process and provided theoretical support for rock stability analysis in mining design and construction. Using laboratory test methods, Xue et al. [13] utilized a high-accuracy automatic testing machine with a controllable loading rate and an AE experimental system to detect and locate stratal instability in the laboratory. The results show that the greater the energy released by the AE signal, the more prone to rock burst. In the numerical simulation of AE, Lv et al. [14] used RFPA2D software to study the compressive strength, crack generation and propagation, and failure mode of coal with combined defects. According to the distribution characteristics of the AE energy of combined coal simulated by RFPA2D software, the failure process of coal with combined defects was analyzed. Based on the cohesive zone model in ABAQUS, Meng et al. [15] studied the influence of bedding plane properties on rock strength, fracture, and AE characteristics.

Most of the above scholars' research contents are based on AE technology to study the damage evolution law of rock. However, there are few AE simulation studies on the surrounding coal mine rock-supporting roadways under dynamic load. Therefore, based on FLAC3D numerical simulation [16–18] software, this study uses numerical simulation and theoretical analyses to study the AE characteristics of the surrounding rock of supporting roadways under dynamic load. Under dynamic loads, the surrounding rock of roadways is often in an unstable state of repeated loading and unloading, and the process of fracture, expansion, and fracture occurs inside. In this process, the rock

produces an AE phenomenon. By detecting the AE phenomenon inside the rock, the unloading failure of the rock can be observed and predicted, which is greatly significant for roadway support design.

2. Numerical Simulation Scheme Design of AE in Supporting Roadways under Different Dynamic Loads

2.1. Numerical Simulation Principle of AE. AE is a phenomenon in that the internal structure of the local part of the rock material is changed under the action of external, which causes the stress redistribution in the rock material, releases energy, and produces transient elastic waves. Its energy conversion is from mechanical energy to acoustic energy. AE is closely related to the generation of cracks in rocks. The expansion and closure of cracks in rocks produce the AE. FLAC3D numerical simulation software has significant advantages in simulating the mechanical properties of a rock mass. By constructing the model, the constitutive relationship is given to the model so that the model has the mechanical properties of rock. The model causes the fracture of the model unit under the condition of applying an external load, and the model unit releases elastic energy during fracture. In FLAC3D numerical simulation, the function is introduced into the calculation model by Fish language, and the strain energy of the unit is calculated in each operation. The rupture of each model unit releases energy to produce an AE event. In the record of AE events, the history command provided by FLAC3D numerical simulation software creates sampling record variables to sample and store the target object.

2.2. Model Unit Rupture Event Judgment Basis. During the numerical simulation, the generation of AE events is related to whether the elastic energy stored in the model unit is released. Therefore, the elastic energy stored in the model unit is calculated by the following equation:

$$W = \frac{1}{2E}\left[\sigma_1^2 + \sigma_2^2 + \sigma_3^2 - 2\mu\left(\sigma_1\sigma_2 + \sigma_1\sigma_3 + \sigma_2\sigma_3\right)\right], \quad (1)$$

where E is the elastic modulus of the medium, μ is the Poisson's ratio of the medium, and σ_1, σ_2, and σ_3 are the maximum, intermediate, and minimum principal stresses applied by the model, respectively.

In the process of model calculation under dynamic load, the elastic energy in the model unit changes continuously with the calculation time step. As shown in equation (2), if the calculated energy density difference is positive, it represents the energy storage. If it is negative, it represents the energy release of the model unit. At this time, the energy release state of the model unit is recorded as an AE event.

$$\Delta U_e = U_e - U'_e, \quad (2)$$

where U_e is the elastic energy of the existing state of the model unit and U'_e is the elastic energy of the previous state of the model unit.

2.3. Simulation Program. The numerical model herein is based on the actual conditions of the Xinjulong Coal Mine. The study aims to investigate the deformation of the roadway and fracture of the rock mass around the roadway under different dynamic loads applied to different positions of the arched roadway under supporting measures and its AE characteristics. The arch tunnel model is established by FLAC3D numerical simulation software, and the Mohr–Coulomb constitutive model is provided. The Fish language is compiled to add a bolt-cable support structure to the roadway model (Figure 1). To study the deformation of the supporting roadway and the fractured state of the rock around the roadway under different dynamic loading conditions, the dynamic loads with the energy values of 1×10^3, 1×10^4, 1×10^5, and 1×10^6 J are applied at different positions of the model end face. As for the location selection of the dynamic load, the above, upper left 45°, and horizontal directions of the model are selected, and a 10×10 m dynamic load is applied in the middle of the model at the above position (Figure 2).

Observing the AE phenomenon within the rock around the roadway by numerical simulation and predicting the deformation of the roadway surrounding rock have certain practical significance in studying the roadway support and controlling the deformation of the surrounding rock.

3. Model Establishment, Parameter Selection, and Dynamic Load Application Criteria

3.1. Establishment of Numerical Model. Herein, FLAC3D numerical simulation software is selected to establish an arch roadway model with a model size of 50 m $\times 50$ m $\times 50$ m. The boundary of both sides of the model is set as a horizontal simple support constraint, and the horizontal displacement of the boundary on both sides is fixed. The lower boundary is set as a fixed support constraint to fix its horizontal and vertical displacements, and the upper boundary applies a uniform load according to the buried depth condition. The model grid is divided by the embedded cylindrical and rectangular roadway radial gradient rectangular grids. Two problems are studied herein. One is the influence of the dynamic load energy at different sizes on the AE characteristics of the supporting roadway model. The second is the influence of the dynamic load energy at different positions on the AE characteristics of the model.

3.2. Parameter Analysis. After dividing the grid unit, the FLAC3D model can provide different lithological mechanical characteristics of the unit. According to the actual geological conditions and lithology borehole histogram, the model is given siltstone and fine sandstone from top to bottom (Figure 3). The mechanical parameters of rock mass are presented in Table 1.

3.3. Dynamic Load Application Criterion. The magnitude of the dynamic load applied in the model is determined according to the relationship proposed by A. McGarr [19] between the peak particle velocity, the distance R from the source center to the dynamic impact damage point, and the rockburst intensity.

$$\lg(\mathrm{Rv}) = 3.95 + 0.57 M_L, \tag{3}$$

$$\lg E_L = 1.8 + 1.9 M_L, \tag{4}$$

where R is the distance from the dynamic load location to the monitoring point (unit: cm) and V is the peak velocity of the surrounding rock vibrating particle detected by the monitoring point (unit: cm/s). The unit of Rv is cm^2/s, E_L is the unit of energy size J, and M_L is the magnitude.

According to equations (3) and (4), it is deduced that

$$v = \frac{10^{3.41 + \lg E_L}}{R}. \tag{5}$$

In FLAC3D, the dynamic load is applied to the model by calling the Fish function, and the dynamic load arrangement of the interface source is used to apply the dynamic load with an area of 10 m $\times 10$ m on the end face of the model. To facilitate the analysis, the dynamic load stress wave is simplified as a section of the cosine wave harmonics. According to the different distances and positions of the source, it is applied to the roadway model, and the vibration period is 0.1 s. To ensure that the energy of the applied dynamic load is within the scope of the scheme design, the relationship between the velocity, distance, and energy of equation (5) is used to achieve different source strength characteristics by setting different source velocities $V_{\max}$. To ensure that the applied dynamic load is within the scope of the design scheme, the survey line is set on the roadway surface, and the velocity of the source stress wave reaching the surface of the roadway is measured to determine the size of the applied dynamic load. The measuring line arrangement is shown in Figure 4. The corresponding relationship between the parameters taken by different intensity dynamic loads and the source distance is shown in Table 2.

4. Simulation Result Analysis

4.1. Application of Dynamic Load Directly above the Model. As shown in Figure 5, when the dynamic load is applied above the end face of the model, the dynamic load of 1×10^4, 1×10^5, and 1×10^6 J is applied, respectively, and the AE distribution map under the three conditions is obtained. According to the AE distribution map, the following analysis is conducted.

As shown in Figure 5(a), when a dynamic load with the energy of 1×10^4 J is applied directly above the model, several four-party AE events are gathered on the end face directly above the model. From the distribution of the AE events, the energy of the dynamic load is transferred from the upper direction of the model to the surrounding roadway. As the dynamic load energy is transmitted in the form of waves, the energy passes through the rock strata of different lithologies in the transfer process, and the energy is attenuated. When the fourth power energy is transferred to the roadway, the energy has been attenuated to the third power energy, so there are few fourth power energy events around the roadway. From the 3D
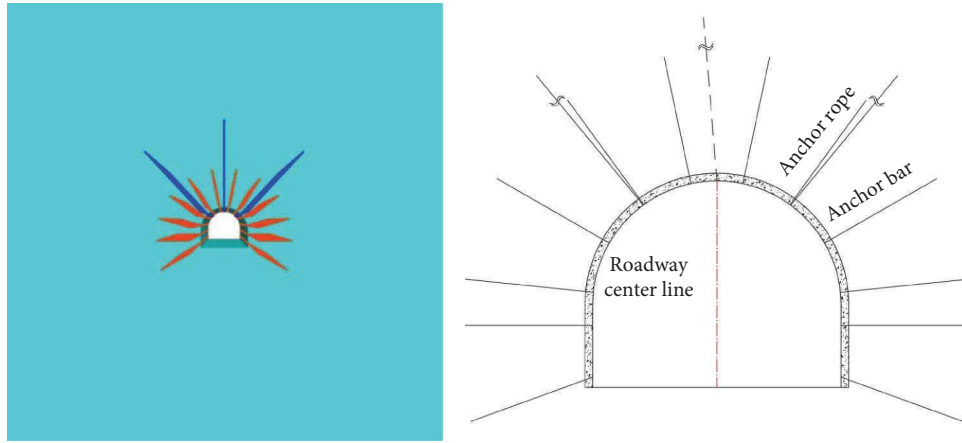
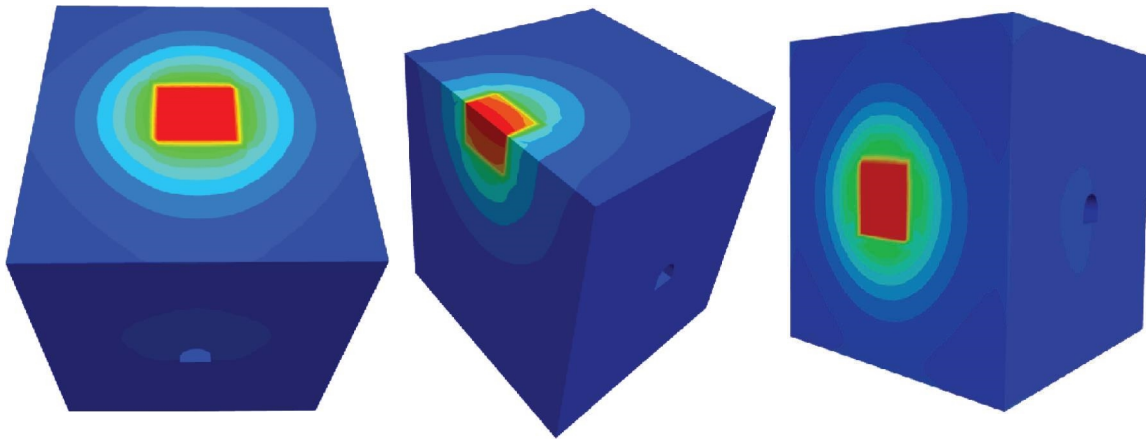Figure 1: Numerical simulation model diagram of roadway support.

Figure 2: Numerical simulation diagram of dynamic load application position.
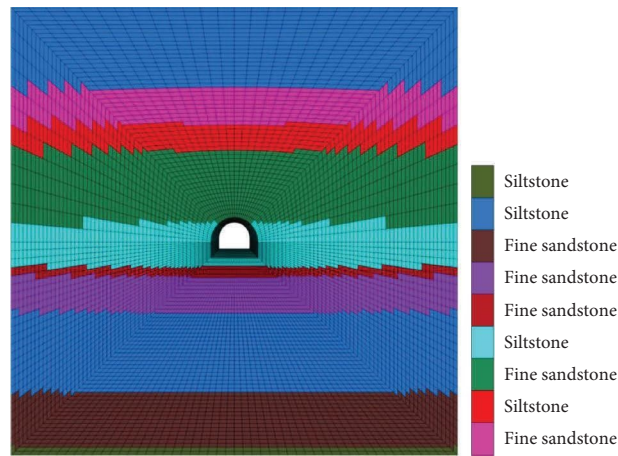

Figure 3: Model layer lithology diagram.

Table 1: Mechanical parameters of rock mass.

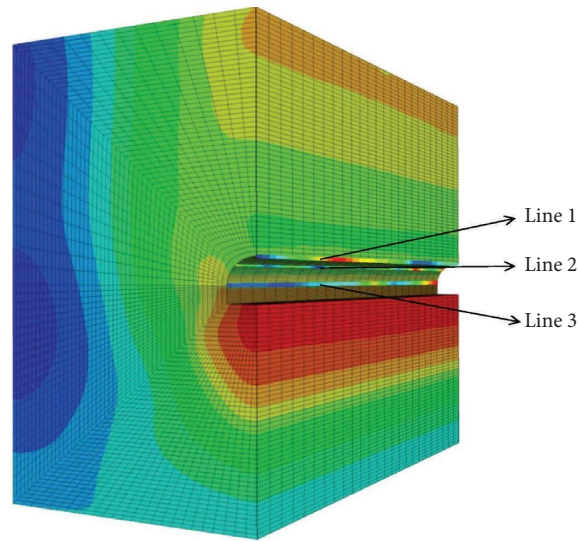|	Density (kg·m^{-3})	Bulk modulus (GPa)	Shear modulus (GPa)	Angle of internal friction (°)	Tensile strength (MPa)
Siltstone	2.75	8.10	4.84	35.7	3.41
Fine sandstone	2.7	7.87	3.38	38.8	5.79

Figure 4: Line layout diagram.

Table 2: Dynamic load intensity and source distance parameters.

Energy of source	Hypocentral distance (m)	Line monitoring peak velocity (v_{max}, unity: m·s^{-1})
1×10^3–1×10^4 J	23.45	0.17
	33.49	0.12
	22.35	0.18
1×10^4–1×10^5 J	23.45	0.35
	33.49	0.24
	22.35	0.36
1×10^4–1×10^5 J	23.45	0.69
	33.49	0.48
	22.35	0.73

distribution state of the AE events, the number of AE events in the middle of the roadway is relatively denser than at both ends of the roadway because the dynamic load is applied directly above the middle of the roadway. Due to the barrier effect of the roadway on the dynamic load stress waves, the AE events near the roadway floor are few, but the AE events at the roadway bottom angle are many, and the energy of the AE events is less than the fourth power. Therefore, the tunnel bottom angle support should be strengthened in engineering construction.

Figure 5(c) shows the case where a dynamic load with the energy of 1×10^5 J is applied above the model. As the applied dynamic load energy increases, the number of AE events significantly increases. During the dynamic load energy transfer process, the fifth power dynamic load energy also decayed, and from the AE event distribution state, the fifth power energy events were mainly distributed above the model, which was the same as the case of applying the fourth power dynamic load energy. According to the 3D distribution state of the AE events, the AE events with the third power energy are mainly distributed around the roadway, and the distribution state of the AE energy in the middle of the roadway and near the floor is similar to the case when the fourth power dynamic load is applied.

Figure 5(c) shows the case where a dynamic load with the energy of 1×10^6 J is applied above the model. The transfer path of the dynamic load energy is the same as that of the fourth and fifth power dynamic load energy. However, on the transfer path of the dynamic load energy, most of the AE events on the transfer path with the sixth power dynamic load energy are the fifth power energy. From the 3D distribution state of the AE events, several AE events with the fifth and fourth power energies appear around the roadway, indicating that under the dynamic load disturbance of the sixth power energy, the model elements around the roadway release elastic strain energy greater than the fourth power energy. The AE event distribution in the bottom angle area of the roadway is similar to the dynamic load with the fourth and fifth power energy, but the AE of the model with the dynamic load with the sixth power energy exceeds the third power energy, which is related to the dynamic load energy applied by the model.

4.2. Dynamic Load Applied 45° from Top Left of Model.
As shown in Figure 6, in the upper left of the model end face 45° direction were applied to 1×10^4 J, 1×10^5 J, and 1×10^6 J dynamic load case, the propagation path of the dynamic
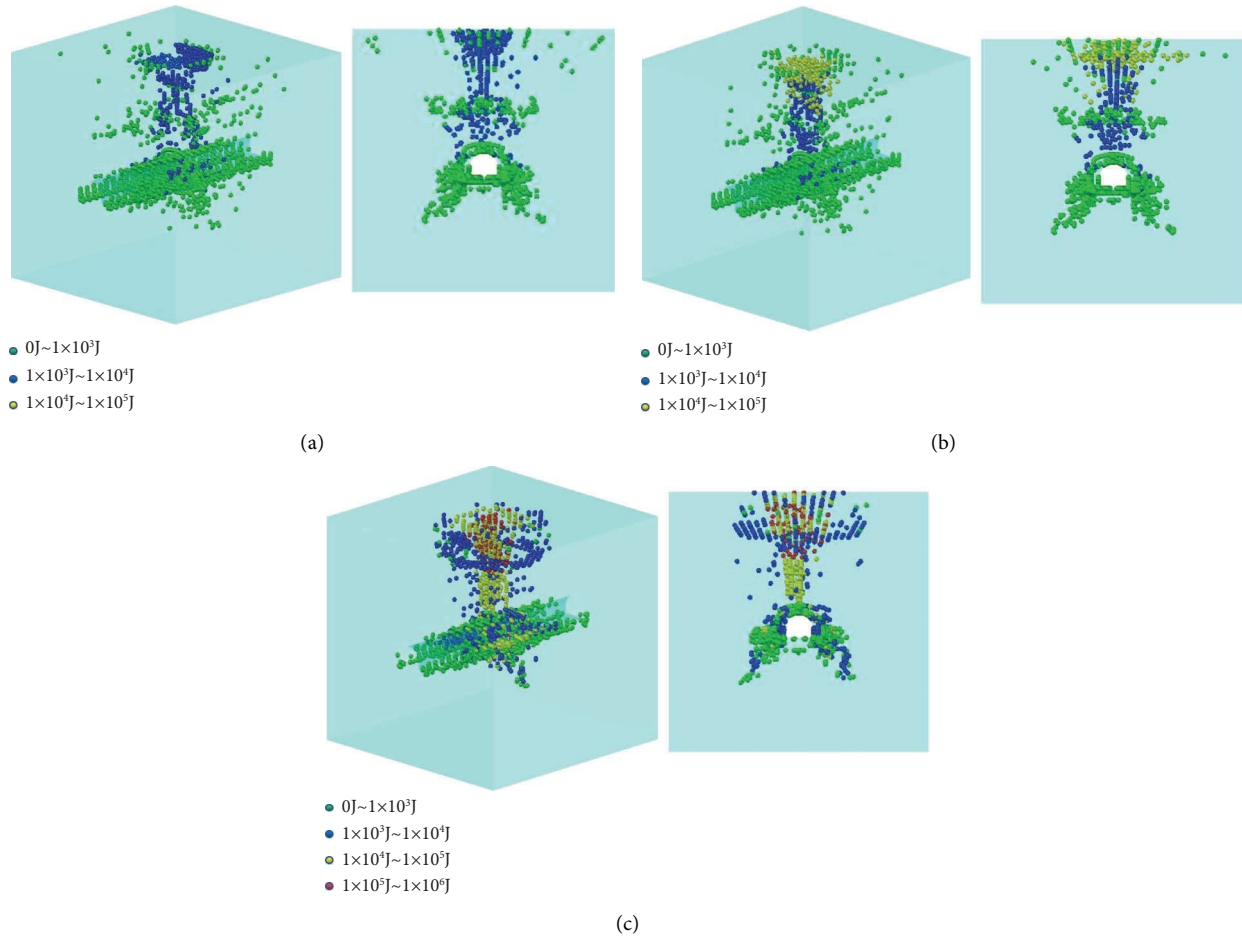
(c)

FIGURE 5: Distribution state diagram of acoustic emission right above the model. (a) State distribution diagram of four-power dynamic load energy acoustic emission. (b) State distribution diagram of five-power dynamic load energy acoustic emission. (c) State distribution diagram of six-power dynamic load energy acoustic emission.

stress wave is almost the same. However, the dynamic load of different energies induced by distributing the AE events is very different.

As shown in Figure 6(a), when a dynamic load energy of 1×10^4 J is applied at 45° above the left of the model, several four-power energy events appear near the dynamic load source and propagate down to the surface of the tunnel, indicating that a large amount of elastic strain energy stored inside the model element is released under the applied dynamic load disturbance. During the energy transfer, the energy is greatly attenuated by the influence of the distance and model layer, which is similar to the case of applying the dynamic load directly above the model. From the perspective of the AE distribution, the roadway is surrounded by many AE events of cubic energy. The number of AE events in the middle of the roadway greatly exceeds that at both ends of the roadway because the dynamic load position is projected in the middle of the roadway, and the distance from both ends of the roadway to the dynamic load source is farther.

As shown in Figure 6(b), when a dynamic load energy of 1×10^5 J is applied at 45° above the left of the model, the dynamic load source area mostly reaches the fifth power energy. However, compared with the AE events of the fourth

power, the AE events of the fifth power are still relatively few, indicating that the dynamic load energy of the fifth power does not induce most of the AE events of the fifth power. In the energy transfer path, the most distribution is the fourth power energy of the AE events, and the energy transfer process also occurred in the inevitable attenuation. From the distribution of the AE events, there are four square energy AE events around the roadway, which shows that the dynamic load of the five square energy makes the model unit around the roadway break, thus inducing the model unit to release four square elastic strain energy.

As shown in Figure 6(c), the dynamic load energy of 1×10^6 J is applied at 45° above the left side of the model. As the applied dynamic load energy increases, the energy of the AE event in the dynamic load source area reaches the energy of the sixth power. There are many AE events with more than the fourth power energy on the energy transfer path, indicating that the dynamic load of the sixth power energy induces a larger range of small energy AE events. The several fourth power energy AE events also appeared on the surface of the tunnel, indicating that the greater the applied dynamic load energy, the more the energy that can induce AE events will also increase.

● 0J~1×10³J
● 1×10³J~1×10⁴J
● 1×10⁴J~1×10⁵J

(a)

● 0J~1×10³J
● 1×10³J~1×10⁴J
● 1×10⁴J~1×10⁵J

(b)

● 0J~1×10³J
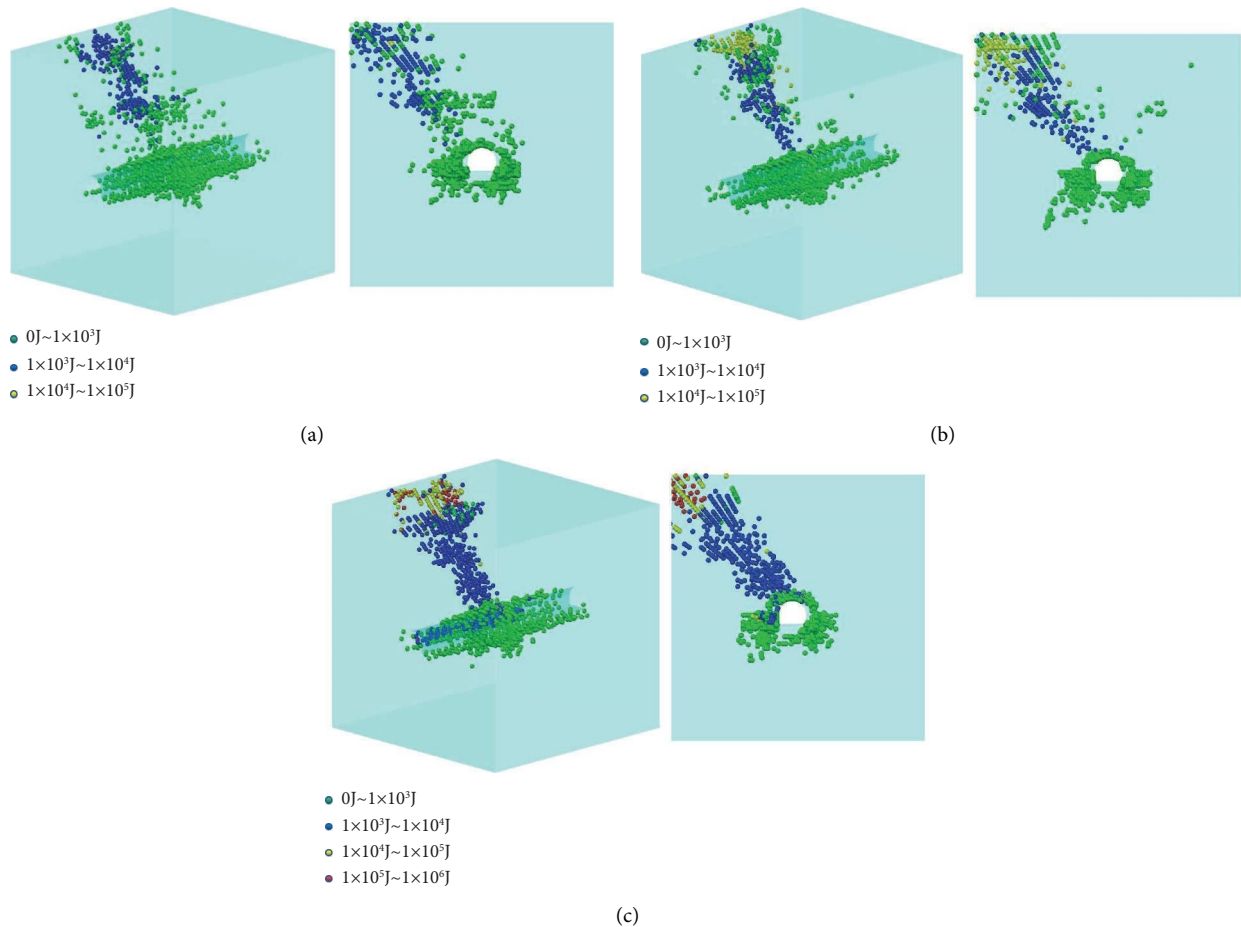● 1×10³J~1×10⁴J
● 1×10⁴J~1×10⁵J
● 1×10⁵J~1×10⁶J

(c)

FIGURE 6: Distribution state diagram of acoustic emission at 45° upper left of the model. (a) State distribution diagram of four-power dynamic load energy acoustic emission. (b) State distribution diagram of five-power dynamic load energy acoustic emission. (c) State distribution diagram of six-power dynamic load energy acoustic emission.

4.3. Model Applying Dynamic Load Horizontally. As shown in Figure 7, when the dynamic loads of 1×10^4, 1×10^5, and 1×10^6 J are applied in the horizontal direction of the model, according to the distribution state diagram of the AE events, the transmission path of the dynamic load stress wave is transmitted from the horizontal direction to the roadway. In addition, because the dynamic load stress wave is transmitted in the same layer during transmission, the propagation of the dynamic load energy is less affected by the lithology of the rock layer.

As shown in Figure 7(a), when the applied dynamic load is the fourth power, the AE events on the dynamic stress wave transmission path are mainly the fourth power, but there are some AE events with energy exceeding the fourth power. This may be because the rock on the dynamic stress wave propagation path breaks under the action of the dynamic-static load coupling, thereby releasing energy to produce AE events with energy exceeding the fourth power. Around the roadway, the AE events are mainly dominated by three square energy events, and the AE events of the fourth power energy are mainly distributed in the middle of the roadway. At both ends of the roadway, the number of AE events is small.

As shown in Figure 7(b), when the applied dynamic load is the fifth power, the AE events on the stress wave transmission path of the dynamic load are mainly the fifth power dynamic load energy. The model unit is subjected to the dynamic–static load coupling. Like the application of the fourth power dynamic load energy, the model applying the fifth power dynamic load energy also has AE events that exceed the fifth power energy on the dynamic load stress wave propagation path. The AE events gathered in the middle of the roadway are mainly the dynamic load energy of the fourth and fifth powers. The number of AE events at both ends of the roadway is small, most of which are the dynamic load energy of the third power.

As shown in Figure 7(c), when the applied dynamic load is the sixth power, the AE events on the transmission path of the dynamic load stress wave are mainly the sixth power dynamic load energy, and the AE events in the middle of the roadway are mainly the fourth and fifth power dynamic load energy. The number of AE events at both ends of the roadway is similar to that of the model that applied the fourth and fifth power dynamic loads.

- 0J~1×10³J
- 1×10³J~1×10⁴J
- 1×10⁴J~1×10⁵J

(a)

- 0J~1×10³J
- 1×10³J~1×10⁴J
- 1×10⁴J~1×10⁵J
- 1×10⁵J~1×10⁶J

(b)

- 0J~1×10³J
- 1×10³J~1×10⁴J
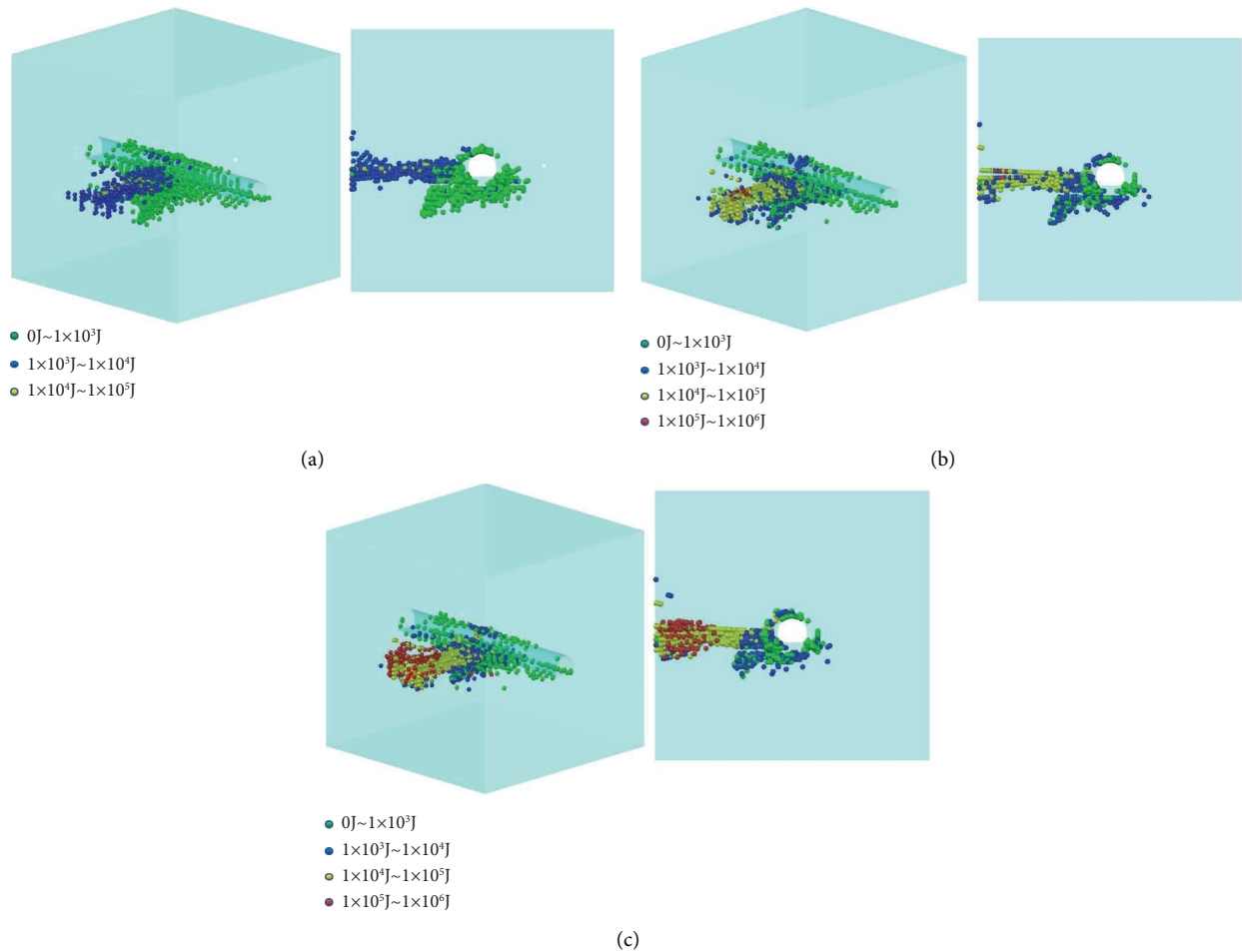- 1×10⁴J~1×10⁵J
- 1×10⁵J~1×10⁶J

(c)

FIGURE 7: Distribution state diagram of horizontal acoustic emission of the model. (a) State distribution diagram of four-power dynamic load energy acoustic emission. (b) State distribution diagram of five-power dynamic load energy acoustic emission. (c) State distribution diagram of six-power dynamic load energy acoustic emission.

5. Conclusion

Through numerical simulation, this paper explores the AE characteristics of supporting roadways when different dynamic load energy values are applied at different positions. According to the theoretical analysis, the following conclusions are drawn:

(1) The strength and distance of the dynamic load source directly impact the AE events. When the dynamic load energy is applied to the end face of the model, the AE energy events near the source location are larger, and the AE events are denser. However, in the propagation path of the dynamic stress wave to the roadway because the dynamic stress wave passes through the rock strata of different lithologies during transmission, the energy attenuates during propagation. Therefore, the AE events near and around the roadway are mainly small energy, and the AE events in the middle of the roadway are denser than those at both ends of the roadway.

(2) When the dynamic stress wave propagates in the rock strata of the same lithology, the energy attenuation of the AE event is smaller than that in the rock strata of different lithologies, and the AE event is more concentrated.

(3) The roadway has a barrier effect on the dynamic load stress wave. According to the 3D distribution state diagram of the AE, when the dynamic load stress wave passes through the roadway, the number of AE events on the other side of the roadway decreases sharply, especially when the dynamic load is applied directly above the model and 45° on the left. According to this phenomenon, roadways are arranged in mines prone to mine earthquakes, and high-level measure roadways can be constructed above the roadways to protect the roadways.

(4) The dynamic load source above the roadway induces the deformation and failure of the bottom angle of the roadway, resulting in the instability of the surrounding rock structure of the roadway.

Therefore, the bottom angle support of the roadway should be strengthened in the process of roadway support.

Data Availability

The data in the manuscript were obtained by experiments and were effectively collected and correctly presented. Data used to support the findings of this study are included in the article.

Conflicts of Interest

The authors declare that they have no conflicts of interest.

Authors' Contributions

The work presented herein was carried out in collaboration between all the authors. Zhigang Liu and Wenzheng Shang proposed the innovative points and wrote the paper. Wenzheng Shang and Wuchao You carried out numerical simulation tests. Jianbo Yuan, Lei Yu, and Shihua Zhang contributed to the design. Shang Wenzheng and Han Shuai contributed to the writing.

References

[1] M. Lin, C. Gao, Y. Xia, D. Zhang, X. Liu, and X. Liang, "Rock burst initiation and precursors in a model specimen based on acoustic emission and infrared monitoring," *Arabian Journal of Geosciences*, vol. 15, no. 4, 2022.

[2] Y. Chen, J. Zhang, J. Chen, and X. Deng, "Special issue: rock burst disasters in coal mines," *Energies*, vol. 15, p. 4846, 2022.

[3] M. Xu, K. Li, and Y. Xu, "Partitioning control mechanism and engineering practice of rebuilding bearing arch in surrounding rock under high ground stress," *Advances in Civil Engineering*, vol. 2021, Article ID 6667182, 9 pages, 2021.

[4] C. Yuan, W. Wang, and C. Huang, "A study on the mechanism and controlling techniques of roadway deformations under high in situ stress conditions," *Geotechnical and Geological Engineering*, vol. 38, no. 1, pp. 605–620, 2020.

[5] R. Peng, R. Xue, H. Sun, and H. Zhou, "Characteristics of strong disturbance to rock mass in deep mining," *Journal of China Coal Society*, vol. 44, no. 5, pp. 1359–1368, 2019.

[6] M. S. Gao, Y. C. Zhao, Y. Y. Wen, Z. C. Cheng, and X. C. Quan, "Stress and energy criterion of the roadway destruction subjected to disturbance type rock burst and its practice," *Meitan Xuebao/Journal of the China Coal Society*, vol. 41, no. 4, pp. 808–814, 2016.

[7] K. Du, X. Li, M. Tao, and S. Wang, "Experimental study on acoustic emission (AE) characteristics and crack classification during rock fracture in several basic lab tests," *International Journal of Rock Mechanics and Mining Sciences*, vol. 133, Article ID 104411, 2020.

[8] T. Jie, S. Zhaoyang, W. Zaihai, and N. Fangbo, "Experimental study on acoustic emission frequency characteristics of granite under different cyclic loading and unloading," *IOP Conference Series: Earth and Environmental Science*, vol. 619, Article ID 012018, 2020.

[9] N. Li, L. Fang, B. Huang et al., "Characteristics of acoustic emission waveforms induced by hydraulic fracturing of coal under true triaxial stress in a laboratory-scale experiment," *Minerals*, vol. 12, p. 104, 2022.

[10] S. Zhili, J. Shengguo, X. Wenbing, and T. Qingteng, "Research on coal acoustic emission characteristics and damage evolution during cyclic loading," *Frontiers in Earth Science*, vol. 10, 2022.

[11] X. Su, H. Ji, D. Quan, T. Zhang, Z. Zhang, and J. Li, "Evolution of the circumferential axial strain ratio and acoustic emission response of loaded rocks," *Arabian Journal of Geosciences*, vol. 15, no. 3, 2022.

[12] J. Yang, K. Zhao, Y. Song et al., "Acoustic emission characteristics and fractal evolution of rock splitting and failure processes under different loading rates," *Arabian Journal of Geosciences*, vol. 15, no. 3, 2022.

[13] J. Xue, Z. Chen, Y. Li, J. Wang, and X. Li, "Failure characteristics of coal-rock combined bodies based on acoustic emission signals," *Arabian Journal of Geosciences*, vol. 15, no. 2, 2022.

[14] H. Lv, Z. Cheng, Y. Dong, J. Zhang, and Y. Ma, "Numerical simulation on the crack initiation and propagation of coal with combined defects," *Structural Engineering and Mechanics, An International Journal*, vol. 79, no. 2, pp. 237–245, 2021.

[15] Y. Meng, H. Jing, X. Liu, Q. Yin, and X. Wei, "Experimental and numerical investigation on the effects of bedding plane properties on the mechanical and acoustic emission characteristics of sandy mudstone," *Engineering Fracture Mechanics*, vol. 245, Article ID 107582, 2021.

[16] X. Li, H. Li, Z. Yang, X. Wang, and W. He, "Numerical simulation case study by using FLAC-3D of the composite coal-rock on the load-free fracture," *Journal of Safety and Environment*, vol. 20, no. 6, pp. 2187–2195, 2020.

[17] D. Xia, K. Leng, Z. Zhang, and Y. Hou, "Research on surrounding rock stability and layout scheme of soft rock roadway based on FLAC3D," *Ming Research and Development*, vol. 40, no. 12, pp. 92–99, 2020.

[18] G. J. Liu, S. L. Li, Z. L. Mu et al., "Numerical study on the impact instability characteristics induced by mine earthquake and the support scheme of roadway," *Shock and Vibration*, vol. 2021, Article ID 7697905, 16 pages, 2021.

[19] G. F. Wang, L. M. Dou, Z. L. Li, S. Gong, J. He, and W. Cai, "Anti-impact abilities calculation and feasibility analysis of seismic reverse for supporting," *Chinese Journal of Rock Mechanics and Engineering*, vol. 34, pp. 4125–4131, 2015.